

# Wavelet thresholding Genetic algorithm approach for Noise Extraction in High-Resolution Industrial Tomography

Ivan B Silva, Mariane R. Petraglia, Antonio Petraglia

Program of Electrical Engineering, COPPE, Federal University of Rio de Janeiro, CP 68504 - CidadeUniversitária, 21945-970, Rio de Janeiro, Brazil

Received: 24 Aug 2020; Received in revised form: 27 Oct 2020; Accepted: 1 Nov 2020; Available online: 7 Nov 2020

©2020 The Author(s). Published by AI Publications. This is an open access article under the CC BY license

(<https://creativecommons.org/licenses/by/4.0/>).

**Abstract**—Since the development of Computed Tomography (CT) in medicine, many applications have been emerging among which the use in Non-Destructive Evaluation (NDE) approach has been consolidating in recent years for analysis of inner features in a broad range of industrial components. More recently, this method has also been applied for dimensional measurements in the metrology field. During acquisition stage many artifacts may cause distortions that interfere with the sample edge evaluation, thereby generating errors on the surface determination. In such development, high accuracy is required for its use in metrology and overall volumetric reconstruction. Scatter radiation is a major concern in the image acquisition process, being strongly dependent on the object densities and geometry. A combined approach involving genetic algorithm and wavelet shrinkage is proposed for denoising application, where 2D radiographic projections are filtered prior to the volumetric reconstruction process. The developed algorithm is applied to sample images resulting from tomography procedures that usually produce severe artifacts and is evaluated in terms of Peak Signal-to-Noise Ratio (PSNR). The filtering technique advanced in this paper generates reconstructed volumes with less noise, accurate edges and improved visual perception.

**Keywords**—Computed Tomography, Denoising, Genetic Algorithm, Wavelet.

## I. INTRODUCTION

The availability of objects built volumetrically through Computed Tomography (CT) in industry has brought product development and material evaluation to a new level, thereby leveraging the comprehension of material behavior in fabrication process. Notably, the CT approach enhances the knowledge about volumetric spread of discontinuities, porous patterns, inclusions, shrinkages, voids and flaws. In addition, it can also compare casted object with the projected model, aiming at correcting discrepancies and improving the casting chain.

In industrial field, usually the most used system is the so-called ConeBeam Computed Tomography (CBCT)[1], in which a x-rays tube generates a cone beam that penetrates the object projecting an image onto a Digital Detector Array (DDA). This technique increases the acquisition speed if compared to traditional medical fan beam CT, since it can acquire images in a larger area.

However, reducing the acquisition time benefit has the downside of increasing artifacts caused by additional scattered radiation. It is well known that the scattered radiation creates undesired secondary signals, which are responsible for generating spurious components in the CT volume.

A number of different techniques and methods for the suppression of scatter-related artifacts have been proposed, and can be software based only [2], [3], or a combination of hardware and software approaches [4],[5]. The artifacts in industrial CBCT turn out to be more severe than those found in medical fan beam CT, since the industrial components present relatively higher density materials, more complex geometries and due to the bigger acquisition area, more exposed to scatter radiation. Based on these considerations, in this work we propose a combined method for filtering these scatter radiations prior to volume reconstruction, by using wavelet shrinkage [6] while

selecting the wavelet family and its parameters through a genetic algorithm [7] for each acquired image.

## II. METHODS

The CBCT acquisition process consists in acquiring thousands of 2D radiographic projections. The sample object is rotated between the x-rays source and the DDA detector. Each image corresponds to a certain angle. After the acquisition phase, the acquired images are submitted to a reconstruction algorithm which creates the sample digital volume. During the acquisition phase, the DDA detector not only acquires the useful penetrated x-rays, but also the scattering coming from deviated, reflected, diffracted x-rays passing through the object and around it. These scattered x-rays produce false information on the reconstructed volume that will degrade image quality, and may cause artifacts, therefore yielding false defect detection analysis.

The approach developed in this work employs a genetic algorithm to determine the parameters in the noise subtraction method by Wavelet Thresholding (WT). Donoho and Jonhstone [8] presented a method for reconstructing the data of a function contaminated by noise. In this approach, a suitable threshold value is chosen such that wavelet noise coefficients can be discarded. If the chosen threshold value is small, then the estimated signal may still contain noise power, and if the chosen threshold is too large the signal is over smoothed. Finding the optimal threshold value is important in order to achieve the best denoised image.

The wavelet shrinkage function determines how the thresholds are applied to the data. There are two basic wavelet shrinkage functions: the soft and hard thresholding. The hard thresholding approach uses a linear function that keeps only the coefficients above a constant  $\lambda$ , which is normally chosen based on the noise variance. In soft thresholding, on the other hand, the shrinkage operation is accomplished by the non-linear equation

$$thr(h) = \begin{cases} 0 & \text{if } |h| \leq \lambda \\ sign(h)(|h| - \lambda) & \text{if } |h| > \lambda \end{cases}$$

This causes the output to be more smoothed and continuous when compared to the hard threshold. A number of different approaches can be adopted in order to establish the threshold  $\lambda$  [9], [10], [11] and [12].

The proposed algorithm is applied to each acquired image prior to the reconstruction stage. The chromosomes represent the parameters to be used for wavelet decomposition and the coefficient of the wavelet shrinkage

procedure. The following wavelet families were adopted: Haar, Daubechies, Coiflets, Symlets, biorthogonal and reverse biorthogonal [13].

The initial population is chosen randomly, totaling 50 individuals, which are submitted to a selection process known as Universal Stochastic Sampling (USS) [7]. In this process,  $\mu$  equally spaced divisions are used, where  $\mu$  is the number of required selections, in this case the size of the population. The cumulative probability of each individual being chosen based on their fitness is calculated, and copies of these individuals are made according to the above calculated probability and distributed throughout the divisions, so that individuals that have higher fitness are more likely to crossover than do the other ones. To perform crossover, a pair of parents having a predefined probability  $P_c$  is chosen randomly, and from the gene numbers (1, 2, 3 and 4) a random point is chosen, where the genes of the first parent at the chosen point are combined with the last genes of the second parent and vice-versa. An example of this procedure is shown in Fig. 1.

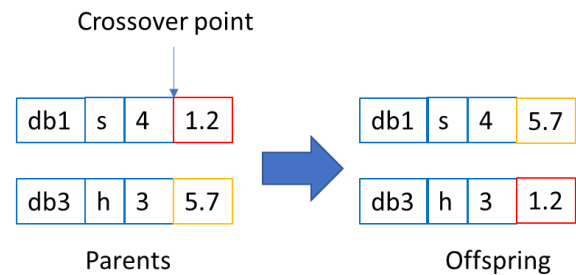


Fig. 1: Crossover illustrative example.

After the crossover, a pair of offspring is generated. These offspring may suffer mutation based on a probability  $P_m$ . The individual selected to undergo mutation has a randomly chosen gene replaced with a possible random value. An example of a mutation can be seen in Fig. 2.

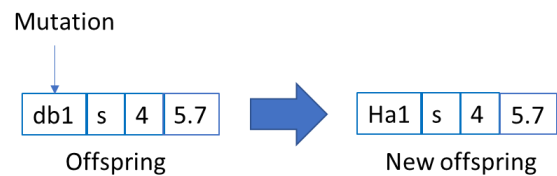


Fig. 2: Mutation illustrative example.

Parents and offspring are evaluated according to the fitness function. The chosen fitness function is the Peak Signal-to-Noise Ratio (PSNR), defined as

$$PSNR = 10 \cdot \log \left( \frac{S_{max}}{\sqrt{MSE}} \right),$$

where  $S_{max}$  is the highest signal strength, given by  $S_{max} = 2^B - 1$ , where B is the number of bits of each pixel representation and MSE is the mean square error between the two images having size  $M \times N$ , that is,

$$MSE = \frac{1}{M \cdot N} \sum_{i=0}^{M-1} \sum_{k=0}^{N-1} \|S_o(i, k) - S_f(i, k)\|^2,$$

where  $S_o(i, k)$  and  $S_f(i, k)$  denote the gray level at the coordinates  $i, k$  regarding the original and filtered images, respectively.

After computing the fitness parameters of all individuals, the one having the highest value is compared to that of the individual that presents the highest fitness value of the previous generation, and the winner is stored. The iteration process is repeated with generation increments up to the generation limit  $G_{max} = 50$ .

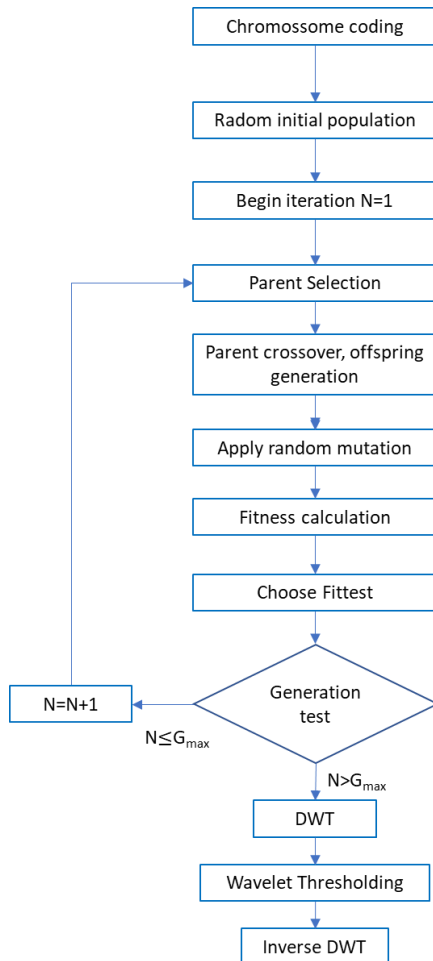


Fig. 3: Flow diagram of proposed algorithm.

Using the fittest parameters, the image is decomposed by applying Discrete Wavelet Transform (DWT) [14], the

coefficients are suppressed accordingly, and the filtered image is obtained from the inverse DWT. The proposed denoising process generates a unique filter for each image, aiming at the best PSNR. The 3D reconstruction process starts after all images are filtered. Fig. 3 presents the flow diagram applied to each projection image.

### III. EXPERIMENTAL RESULTS

In industrial high energy CT different materials and geometries make them difficult to create a standard template to reproduce noise and artifacts found in typical applications. The test specimen employed in this experiment is composed of 3 different materials: stainless steel, aluminum and polyurethane. These materials have very distinct densities and x-ray responses. Moreover, the specimen has parts with different geometries and thicknesses, namely, (a) stainless-steel screw, essentially cylindrical; (b) aluminum and polyurethane sections, with smooth transition geometry; and (c) sections with more abrupt edges. The scans were carried out by employing a CBCT system using a 200  $\mu$ m DDA of 400 mm x 400mm and 4 M pixels, 118 kV, 700  $\mu$ A, 1440 acquired images, 0.5 mm CU filter and 82  $\mu$ m voxel resolution.

The specimen radiography projection is shown in Fig. 4, where the different densities and geometries are evident. A severe noise artifact can be observed in the CT scan of this specimen presented in Fig. 5. This kind of artifact creates a false surface line that leads to a wrong evaluation of the solid, thereby turning accurate metrology impossible. The noise effects can also be observed in cross-sectional images (or “slices”). Figures 6(a) and 6(b) illustrate the illusion of gain and loss, respectively, of material inside the surface line. Also visible in these figures is the presence of beam hardening artifacts.

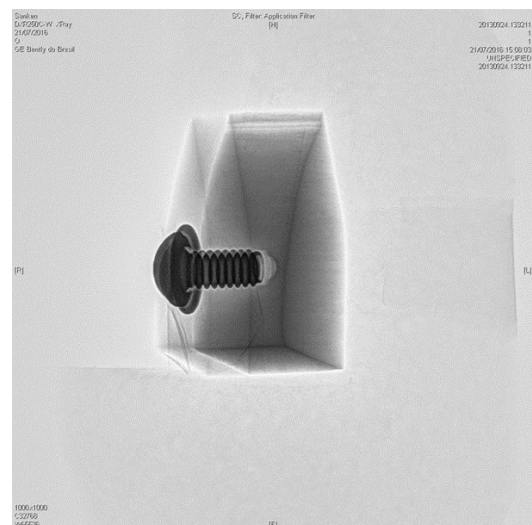


Fig. 4: Specimen 2D radiography.

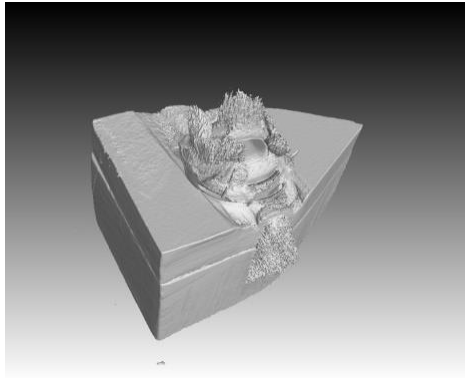


Fig. 5: Specimen CBCT volume result.

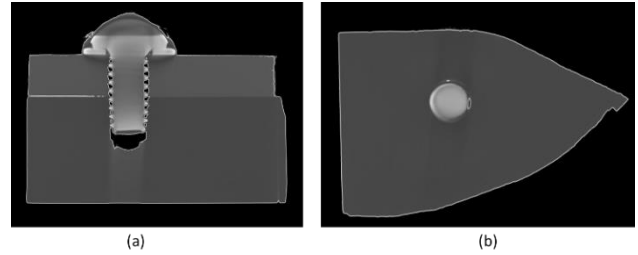


Fig. 8: Slices views obtained from the proposed algorithm: (a) Front view; (b) Top view.

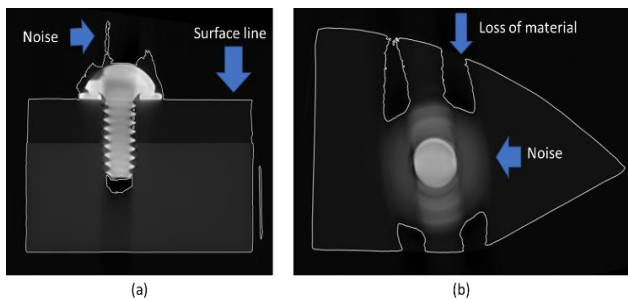


Fig. 6: Slices of the CT scan: (a) Front view slice, with additive noise and line surface indicated; (b) Top view slice, with loss of material and noise around the screw indicated.

The proposed algorithm was applied to each of the 1440 images acquired by the CBCT system. After reconstruction using the Filtered Back Projection algorithm (FBP) [15], the volume generated presented a better visual representation, as displayed in Fig. 7. Figures 8(a) and 8(b) show two slices of the volume in Fig. 7. Compared to the original CT slices (Figs. 6(a) and 6(b)), the surface lines of the resulting images are substantially more accurate, and the gain or loss of material artifacts do not appear so intensely.

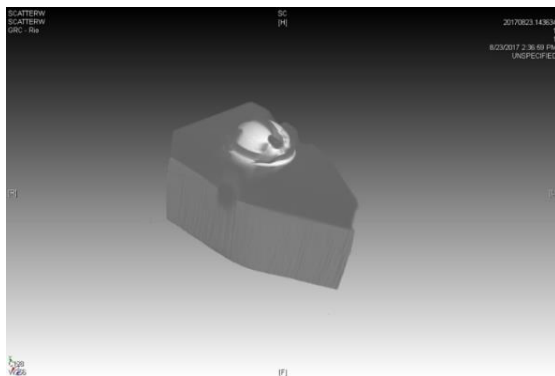


Fig. 7: Test specimen CT reconstruction after filtering by the proposed algorithm.

Fig.9 displays the CT volume colored according to the dimensional deviation measured between the original and the corrected volumes. This analysis shows the areas where the proposed algorithm acted to correct the scattered noise. Green areas represent no or small amount of correction, red areas correspond to additive correction and blue areas show subtractive correction.

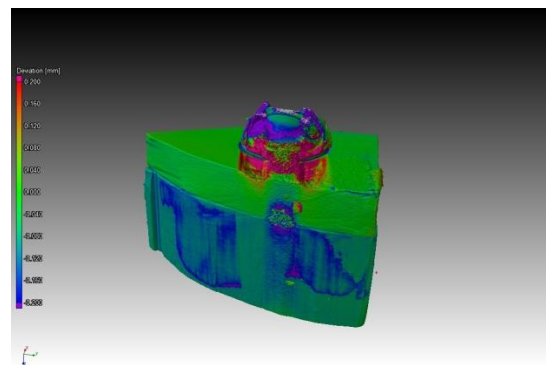


Fig. 9: Comparison between original and filtered volumes using the proposed algorithm.

Differences between the volumes obtained with the original and filtered CT images can be evaluated by comparing the surfaces detected in each volume. Fig. 10 shows the correction statistics applied to the original volume. In this analysis, if both volumes were identical, then the resulting histogram of the dimensional deviations would present only one green peak at 0. Non-zero values at the right-hand side of the zero point indicate that the actual volume contains more material than does the nominal volume in some regions. On the other hand, non-zero values lying at the left-hand side show that the actual volume has less material than does the nominal volume in other regions. As can be observed in Fig. 10, the wavelet denoising approach exhibits excellent performance in regions where subtractive noise contributed more and shows better reduction of the additive noise around the

screw head, which considerably improves the volume quality.

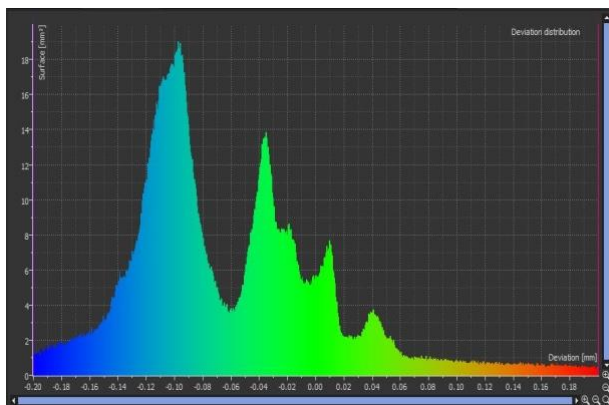


Fig. 10: Histogram of dimensional deviation between original and filtered volumes using the proposed algorithm.

To evaluate the efficiency of the proposed algorithm when compared to other methods, the original volume was also processed with 3 traditional filters, namely, Median [16], Adaptive Gauss [17], and Non-Local Means (NLM) [18]. These three filters were chosen because they are commonly available in commercial CT visualization software and are the most used in noise reduction applications.

The original and filtered volumes were superimposed, and the dimensional deviation histograms calculated. Fig. 11 shows the dimensional deviation histogram for a 3x3 median filter. There was some noise reduction, but the effect was of small amplitude. Fig. 12 displays the dimensional deviation histogram between the original and filtered volumes using adaptive gauss filter. This filtering technique produced a substantial material reduction, thereby resulting in an increase of the original material loss, yielding an undesired opposite effect. It also removed material from the polyurethane part. The histogram profile shown in Fig. 13 represents the dimensional deviation histogram after applying the NLM filter. The form is similar to that of the median filter, but with larger material reduction.

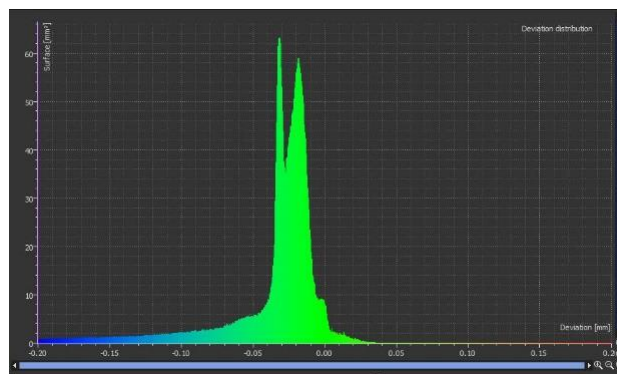


Fig. 11: Histogram of dimensional deviation between original and filtered volumes using Median filter.

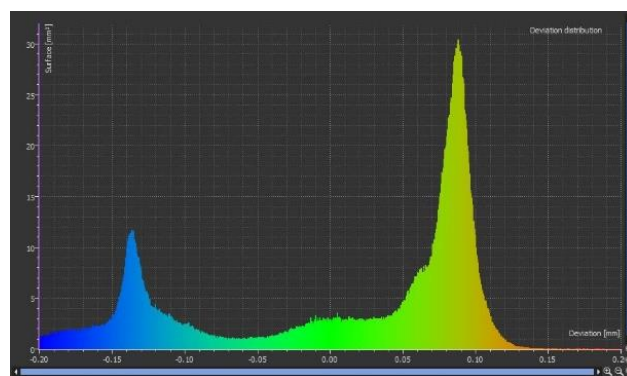


Fig. 12: Histogram of dimensional deviation between original and filtered volumes using Adaptive Gauss filter.

From Figs. 10 to 13, it can be observed that the proposed algorithm showed not only a better performance in correcting both additive and subtractive noise, but also created a more accurate volume with respect to the original object.

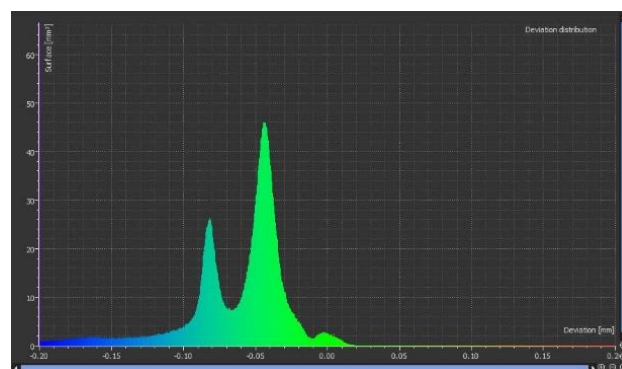


Fig. 13: Histogram of dimensional deviation between original and filtered volumes using NLM filter.

A second dataset was applied in order to analyze the evolution of the noise reduction during an iterative

process, where the dataset, after a generation run, was used as input of sequential generation runs. The sample was an iron casting that produced severe scattering due to its high density and complex geometry. Different from the test specimen, this sample is made of a homogenous material with thicker and denser walls.

Fig. 14 presents the original volume and Fig. 15 shows the evolution after 4 runs. The visual quality improvement can be seen specially in the center of the sample, where in the original volume seemed almost closed. After some runs it is possible to observe the air between the two sides of the sample.

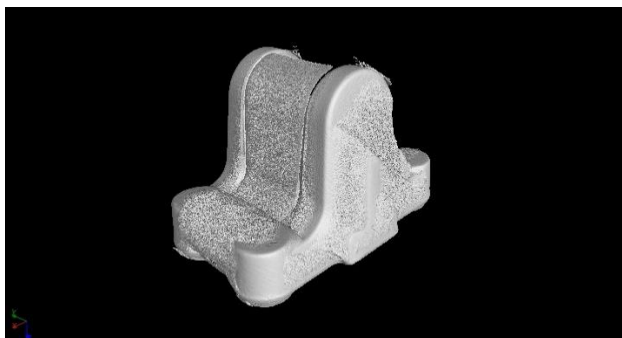


Fig. 14: Iron casting original reconstructed volume.

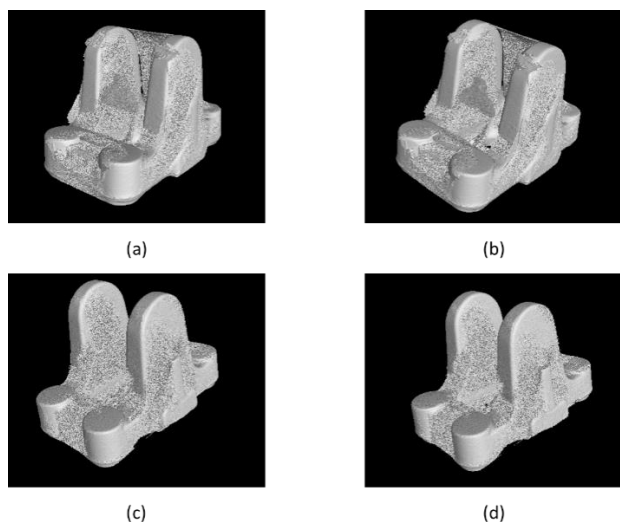


Fig. 15: Evolution of noise reduction.

This same sample was scanned again using a CBCT with the “scatter correct” technology presented by Oliver Brunke[4], which employs a metal grid to measure the scattered radiation during scanning. The measured radiation is, then, subtracted from a second scan without the grid. The result is a better volume with reduced noise power. For each run of the proposed algorithm the gray value histograms of the volumes were computed and then

compared to the gray value histogram of the second scan with “scatter correct” CBCT. The result of all histograms can be seen in Fig. 16.

The left peak of each histogram represents the air in the 3D volume. For an ideal noise free volume, there should be, in addition to air, only a second peak representing the iron and between them a valley, with no other gray level. Analyzing the histograms, the “scatter correct” one shows a deeper valley between air and iron, which represents less noise and a better visual perception and a more accurate surface line definition. The original histogram does not show the iron peak nor a valley separation. The first and second runs result in small improvements with the air peak moving to the left-hand side of the histogram, but the third run made an expressive improvement by moving further the air peak and starting to present a separation valley.

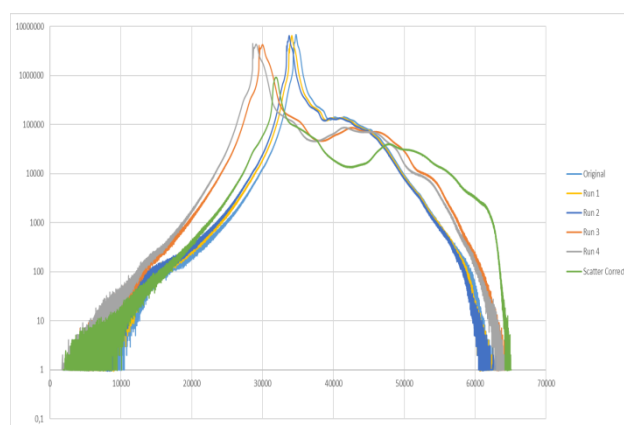


Fig. 16: Gray level histograms of the iron casting.

#### IV. CONCLUSION AND DISCUSSIONS

The wavelet denoising approach parametrized by genetic algorithm generates a customized filter that adapts for each radiographic projection noise profile. A test object created to increase scattered noise by its geometry and different densities was scanned and evaluated by the proposed algorithm. The final visual quality was strongly improved, and the noise power was decreased to such a level that destructive interference was substantially reduced. Not only the overall quality of the reconstructed volume was improved, but also the edge accuracy and surface line determination were significantly enhanced when compared to the original scan.

When compared to traditional smoothing filtering techniques, the proposed algorithm presented better results by reducing material where there was additive noise and regenerating material where there was subtractive noise. This behavior originates from the optimized filters created for each projected image before reconstruction.

The denoising behavior during multiple runs has a stochastic nature due to the GA part of the algorithm, where small improvements can be made or significant noise reduction at different stages can be observed. Although there was an important improvement in reducing noise, some noise power remained around the screw head in the test specimen and in some regions of the iron casting sample.

Different datasets were submitted to the proposed algorithm. The objects scanned differ in shape, material, densities, and noise level. In all studies some amount of noise power reduction and material loss correction were achieved, thereby improving visual perception of the volumes, even in cases where there was just a small amount of noise power in the original volume.

During the development of this project, it was also evaluated whether the proposed algorithm would modify the edges in such a way that accurate features measurements would become unfeasible. Scanning objects with known measured features proved that the use of the algorithm did not induce deviation on the expected detected edges and surface lines.

#### ACKNOWLEDGEMENTS

This work was partially supported by CNPq, FAPERJ, and CAPES, Brazil.

#### REFERENCES

- [1] S. Carmignato, W. Dewulf and R. Leach, *Industrial X-Ray Computed Tomography*, Springer International Publishing AG, 2018.
- [2] F. J. Beekman and W. Zbijewski, "Efficient Monte Carlo Based Scatter Artifact Reduction in Cone-Beam Micro-CT," *IEEE TRANSACTIONS ON MEDICAL IMAGING*, vol. 25, no. 7, 2006.
- [3] N. Bhatia, J. M. Létang, D. Tisseur and F. Buyens, "Scattering Correction in Cone Beam Computed Tomography," in *Digital Industrial Radiology and Computed Tomography*, Belgium, 2015.
- [4] O. Brunke, "A new Solution for Scatter Correction in Industrial Cone Beam Computed Tomography," in *7th Conference on Industrial Computed Tomography*, Leuven, 2017.
- [5] M. Baer, M. Hammer, M. Knaup, I. Schmidt, R. Christoph and M. Kachelriess, "Scatter Correction Methods in Dimensional CT," in *Conference on Industrial Computed Tomography (ICT)*, Wels, 2012.
- [6] D. L. Donoho, "Denoising by Soft-thresholding," *IEEE Transaction on Information Theory*, vol. 41, no. 3, 1995.
- [7] A. Eiben and J. Smith, *Introduction to Evolutionary Computing*, Springer, 2003.
- [8] D. L. Donoho and I. M. Johnstone, "Ideal Spatial Adaptation by Wavelet Shrinkage," *Biometrika*, vol. 81, no. 3, 1994.
- [9] S. A. Ali, S. Vathsal and K. L. Kishore, "CT Image Denoising Technique using GA aided Window-based Multiwavelet Transformation and Thresholding with the Incorporation of an Effective Quality Enhancement Method," *International Journal of Digital Content Technology and its Applications*, vol. 4, no. 4, 2010.
- [10] S. G. Chang, B. Yu and M. Vetterli, "Adaptive Wavelet Thresholding for Image Denoising and Compression," *IEEE TRANSACTIONS ON IMAGE PROCESSING*, vol. 9, no. 9, 2000.
- [11] Y. Fang, Y. Zhou, D. Ge and Z. Zhou, "De-noising Based on Wavelet Analysis and Bayesian Estimation for Low-dose X-ray CT," in *The Ninth International Conference on Electronic Measurement & Instruments*, 2009.
- [12] S. Singh and S. Wadhvani, "Medical Image Denoising Using Sub Band Adaptive Thresholding Techniques Based on Wavelet 2D Transform," *International Journal of Bio-Science and Bio-Technology*, vol. 7, no. 5, 2015.
- [13] A. N. Akansu and R. A. Haddad, *Multiresolution Signal Decomposition*, Academic Press, 2001.
- [14] S. K. Mitra, *Digital Signal Processing - a Computer-based Approach*, McGraw-Hill Education, 2010.
- [15] L. A. Feldkamp, L. C. Davis and J. W. Kress, "Practical cone-beam algorithm," *Journal of Optical Society of America*, vol. 1, no. 6, 1984.
- [16] G. Ilango and B. S. Gown, "  $\epsilon$ -Neighborhood Median Filters to Remove Speckle Noise from CT – Images'," *International Journal of Applied Information Systems (IJAIS)*, vol. 4, no. 10, 2012.
- [17] C. Westin, H. Knutsson and R. Kikinis, *Adaptive Image Filtering*, Handbook of Medical Imaging, Academic Press, 2000.
- [18] A. Buades, B. Coll and J. Morel, "A non-local algorithm for image denoising," in *IEEE Computer Society Conference on Computer Vision and Pattern Recognition*, 2005.